ACS OMEGA

http://pubs.acs.org/journal/acsodf

Article

Rational Design of Self-Supported CuO_x-Decorated Composite Films as an Efficient and Easy-Recycling Catalyst for Styrene Oxidation

Bin Du,* Lili Qiu, Yuting Chen, and Ziqi Zhang

Cite This: *ACS Omega* 2021, 6, 18157−18168

Read Online

ACCESS | Metrics & More | Article Recommendations

ABSTRACT: The applications of graphene-based materials in catalysis are limited by their strong tendency to aggregate, which may lead to a decrease in active sites. Herein, we propose a facile and controllable strategy to fabricate a series of heterogeneous catalysts with a unique nanostructure wherein CuO_x-decorated reduced graphene oxide (rGO) sheets are incorporated into a solid matrix composed of poly(vinylpyrrolidone) (PVP) and carboxymethyl cellulose (CMC). The resultant materials are self-supported films and could be directly used as catalysts for the liquid-phase oxidation of styrene without the requirement for extra substrates. The employment of PVP-CMC (PC) as the support for CuO_x-decorated rGO sheets successfully inhibits their aggregation. Benefiting from the dispersion of copper species, these films exhibit good catalytic activity and recyclability under mild reaction conditions. Especially, they can be conveniently removed from the reaction mixture by tweezers due to their structural stability. For catalyzing multiple reactions with high efficiency and facile recyclability, this study offers a universal strategy to design heterogeneous catalysts based on graphene materials and provides a promising platform.

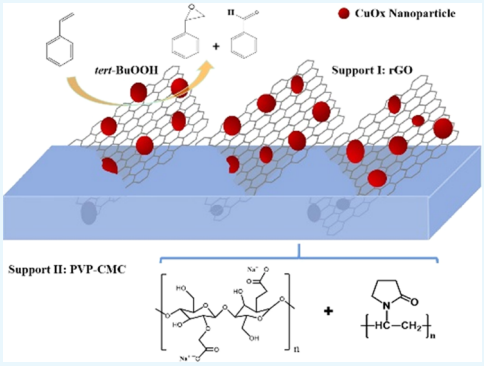

1. INTRODUCTION

Owing to their two-dimensional sp^2 hybrid carbon structures, large surface area, good mechanical strength, and versatile functional groups, graphene and its derivatives can serve as a catalyst support promoting interactions with multiple catalytic species.[1−3] By now, graphene-based catalysts have been frequently employed as heterogeneous catalysts in many reactions, including water splitting, oxygen reduction reaction, Fischer−Tropsch synthesis, selective hydrogenation, catalytic purification of VOCs, oxidation, and so on.[4−6] Compared with the pristine graphene derived from the micromechanical cleavage or chemical vapor deposition (CVD) methods,[7−10] graphene oxide (GO) is more suitable as a catalyst support because of its intrinsic oxygen-doped surface.[11,12] In particular, the oxygen functional groups of GO allow for strong metal-support interactions, which could improve the stability of catalytically active species.[13−15] Usually, the fabrication of graphene-based catalysts is achieved via a wide range of approaches, including thermal, chemical, and hydro-/solvothermal treatments, during which the reduction of GO and deposition of catalytically active species on the basal plane of GO simultaneously occur.[16−18] Nevertheless, due to the presence of the $\pi-\pi$ interaction, the reduced graphene oxide (rGO) sheets are prone to aggregation during the reduction of GO.[19] According to recent reports, the aggregation of graphene-based materials usually leads to a decrease in the availability of catalytically active sites resulting in limitations in the applications of these materials in catalysis.[20,21]

Generally, several strategies are used to prevent the aggregation of graphene-based materials with varying degrees of success.[22−26] Certain polymeric materials, such as PVP, PDDA, and so on, have been used as stabilizing agents to avoid the aggregation of rGO sheets. Recently, Pan et al.[23] reported that in the presence of PDDA, highly dispersed Ag-functionalized graphene nanocomposites could be synthesized via a one-step hydrothermal method. The resultant materials showed high electrocatalytic activity for the oxygen reduction reaction during the energy-saving electrolysis of Na_2CO_3 on account of the absence of agglomeration between Ag NPs and rGO in the presence of PDDA. Pluronic P123 surfactant, a nonionic triblock copolymer, has been used to stabilize Pd@GO nanosheets in aqueous solutions during the oxidation of aliphatic alcohols using a nontoxic oxidant (air).[24] The addition of surfactants remarkably influenced the catalytic activity of Pd@GO by enhancing its dispersity. Hutchings et al.[25] reported the successful synthesis of Au−Pd/graphene oxide/titania "ternary" catalysts with high activity for the selective oxidation of a range of alcohols. Electron diffraction

Received: April 16, 2021
Accepted: June 25, 2021
Published: July 6, 2021

Table 1. Comparison of the Catalytic Performance for Styrene Oxidation Using Different Copper-Based Catalysts[a]

				selectivity [%][g]		
entry	catalyst	Cu content [mmol/g][f]	conv. [%][g]	SO	Bzh	OP
1[b]	commercial CuO		49.3	45.6	38.1	16.3
2[b]	CuO@rGO-PC	2.17	64.6	50.9	32.6	16.5
3[b]	Cu@rGO-PC-25	2.64	65.4	50.5	28.9	20.6
4[b]	Cu@rGO-PC-50	2.02	45.6	48.9	34.0	17.1
5[b]	Cu@rGO-PC-75	1.33	34.3	41.2	47.6	11.2
6[b]	Cu@rGO (powder)	6.41	72.9	47.5	29.1	23.4
7[b]	Cu@rGO (bulk)	6.11	42.5	39.9	48.4	11.7
8[b]	$Cu(NO_3)_2$		41.8	32.5	37.3	30.2
9[c]	PC		24.8	18.2	66.6	15.2
10[d]	rGO		18.7	16.4	66.3	17.3
11[e]	blank		4.1	13.6	70.3	16.1

[a]SO = styrene oxide, Bzh = benzaldehyde, and OP = other products. [b]Reaction conditions: styrene (2.0 mmol), catalyst (1.5 mol % Cu), CH_3CN (5 mL), *tert*-BuOOH (2 equiv), 70 °C, 4 h. [c]Reaction conditions: styrene (2.0 mmol), catalyst (18.0 mg), CH_3CN (5 mL), *tert*-BuOOH (2 equiv), 70 °C, 4 h. [d]Reaction conditions: styrene (2.0 mmol), catalyst (3.0 mg), CH_3CN (5 mL), *tert*-BuOOH (2 equiv), 70 °C, 4 h. [e]Reaction without any catalyst. [f]Cu content in the catalyst, measured by ICP-MS. [g]Conversions and selectivities were determined by GC.

analysis confirmed that GO sheets were dispersed among TiO_2 particles, thus suggesting that the aggregation of GO sheets could be prevented by intercalating titania particles to form ternary hybrid catalysts.

Selective oxidation of alkenes to corresponding epoxides and aldehydes is one of the most significant reactions in organic synthesis since epoxides and aldehydes served as versatile intermediates for the synthesis of agrochemicals, fine chemicals, and pharmaceuticals.[27] Traditionally, stoichiometric inorganic reagents, such as peracid and bromate, have been widely used in the industrial oxidation of alkenes, but they unavoidably produce unwanted products and create a lot of waste requiring purification.[28] Thus, considerable effort has been put into developing efficient catalytic systems using environmentally benign oxidants, such as alkyl hydroperoxide, hydrogen peroxide, or oxygen.[29−32] Copper-based nanocatalysts, which are prepared from inexpensive, naturally abundant, and environmentally friendly copper metal, exhibit remarkable catalytic performance in various reactions.[33,34] Copper surfaces have been shown by Lambert et al. to be selective for the epoxidation of higher alkenes.[35,36] Instead of metallic copper, Cu_2O nanocrystals demonstrated morphology-dependent catalytic activity with O_2 in propylene oxidation.[37] However, these catalysts exhibit high epoxide selectivity with molecular oxygen only at low alkene conversions. In addition to molecular oxygen systems, H_2O_2 and organic peroxides have been shown to notably improve the activity of copper-based nanocatalysts in the selective oxidation of alkenes.[33] However, these nanocatalysts tend to aggregate, resulting in difficulties related to their separation and recovery; such disadvantages prohibit the wider application of these materials to different fields.[38,39] In this work, we employed GO as a precursor to fabricate Cu NPs anchored on rGO (denoted as Cu@rGO) via polyol reduction using ethylene glycol (EG); the obtained materials were then used to catalyze the oxidation of styrene with TBHP as an oxidant.[40] Although the copper loading percentage of Cu@rGO was optimized under the presence of a protective agent (PVP), aggregation of Cu@rGO sheets resulting in the formation of large flakes was still observed. These flakes exhibited obviously lower catalytic activity compared with that of powdered Cu@rGO. Unfortunately, the Cu@rGO powders were obtained with low yields and demonstrated poor recovery properties.

We demonstrate a facile and controllable strategy to fabricate self-supported thin films with a controlled architecture to prevent the aggregation of CuO_x-decorated rGO sheets. In particular, the CuO_x-decorated rGO sheets are incorporated into a composite matrix composed of PVP and CMC. The as-synthesized films, which are denoted as Cu@rGO-PC-*x*, could serve as heterogeneous catalysts for liquid-phase styrene oxidation using TBHP as the sole oxidant under mild conditions. Interestingly, the oxidation of surface copper species of active Cu NPs by TBHP occurs during the reaction, resulting in the formation of copper oxides in the recovered catalyst (denoted as CuO@rGO-PC). Further investigation on the catalytic performance of CuO@rGO-PC demonstrates that the catalytic films possess a truly heterogeneous nature with remarkable catalytic activity, high stability, and good recyclability. It is worth pointing out that conventional catalytic films were usually supported by inert substrates, such as quartz slides and metal foil,[41−46] when they served as heterogeneous catalysts in the catalytic process. Unlike previous conventional catalytic films, our self-supported CuO_x-decorated catalytic films can be cut into small pieces and directly used as catalysts for liquid-phase styrene oxidation. After the required reaction, the pieces can be conveniently removed from the mixture by tweezers. Moreover, the results of scanning electron microscopy (SEM), Fourier transform infrared (FTIR) spectroscopy, and thermogravimetric analysis (TGA) indicate the robust nature of CuO@rGO-PC.

2. RESULTS AND DISCUSSION

2.1. Relationship between the Structure and Catalytic Performance of Cu@rGO-PC-*x*. The catalytic performance of the copper-based catalysts was evaluated via the oxidation of styrene in acetonitrile at 70 °C with 2 equiv of TBHP. In the absence of the catalyst, poor conversion to the desired products was observed (Table 1, entry 15). Following the pioneering work of Bielaswki on the use of GO as a heterogeneous catalyst for liquid-phase oxidation,[47] several other graphene-based materials have been directly employed as carbocatalysts.[48−51] In the present work, oxidation by rGO afforded 18.7% styrene conversion and 82.7% selectivity for the primary products (styrene oxide and benzaldehyde), thereby indicating that rGO could catalyze styrene oxidation under the present conditions. Comparison of the activity of several

https://doi.org/10.1021/acsomega.1c02031
ACS Omega 2021, 6, 18157−18168

copper-based catalysts based on the same Cu mol % with respect to the substrate was conducted; Table 1 lists the Cu contents of the samples determined by ICP-MS. All of the copper-based materials tested showed certain catalytic activity for styrene oxidation. Oxidation by Cu@rGO (powder) gave 72.9% styrene conversion and 76.6% selectivity for the primary products within 4 h; these values are superior to those obtained from rGO. Therefore, copper species, rather than rGO, appear to be the primary active sites in the catalyst. The excellent catalytic activity of Cu@rGO (powder) should be attributed to the dispersion of Cu NPs on the surface of the rGO sheets. When PVP is used as a stabilizer for Cu NPs, its hydrophilic amide groups coordinate with copper through the C−N and C═O groups.[52] Moreover, the polyvinyl backbone of PVP forms a hydrophobic domain that surrounds Cu NPs and inhibits their agglomeration on rGO sheets.[53] Obviously, the spherical Cu NPs were randomly distributed on the rGO sheets in Cu@rGO (powder) (Figure 1a). Statistical analysis

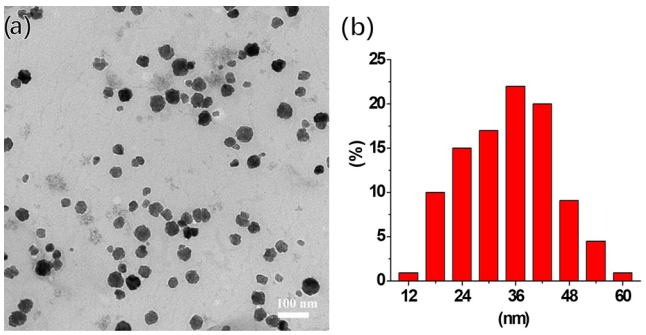

Figure 1. (a) TEM image of Cu@rGO (powder). (b) Particle size distribution of the Cu NPs.

demonstrated that the Cu NPs have a particle size of 18−48 nm (Figure 1b). These results indicate that the addition of PVP can efficiently inhibit the stacking and agglomeration of Cu NPs on the rGO sheets, thereby leading to a decrease in the activity of the former.

As mentioned earlier, the chemical reduction of GO into rGO usually leads to the irreversible restacking of individual graphene sheets. Anchoring catalytically active species onto rGO surfaces has been proven to effectively inhibit the restacking of graphene sheets. CuO_x nanospheres incorporated into the graphene sheets with the help of 3-aminopropyltriethoxysilane (APTES) and PVP could efficiently prevent the graphene sheets from stacking, resulting in a sandwich structure.[54] Bulusheva et al.[55] reported that CuO sheets can act as a spacer to limit the face-to-face aggregation of graphene nanosheets. The microscopic surface topographies of Cu@rGO (powder) and Cu@rGO (bulk) were characterized by SEM. Although typical wrinkled nanosheets were obtained for Cu@rGO (powder) (Figure 2a),[56] the aggregation of Cu@rGO sheets resulted in the formation of large flakes in Cu@rGO (bulk) (Figure 2b).

The presence of these flakes suggests that Cu@rGO aggregation sheets still occur during the synthesis of the material. Achieving the complete dispersion of rigid solids in acetonitrile even under vigorous stirring at the reaction temperature appears to be challenging (Figure 3h). Moreover, the styrene conversion of Cu@rGO (bulk) was considerably lower compared with that of Cu@rGO (powder) under identical reaction conditions (42.5 vs 72.9%, Table 1, entries 2 and 3), thereby indicating the adverse effect of aggregation on the catalytic activity of Cu@rGO (bulk). Cu@rGO (powder) (Figure 3b) could be separated from Cu@rGO (bulk) (Figure 3c) through a sieve, and the weight ratio of Cu@rGO (powder)/Cu@rGO (bulk) was 10.3:100. These results confirm that during the synthesis of the catalyst, incorporation of Cu NPs into the surface of GO in the presence of PVP does not inhibit the aggregation of Cu@rGO sheets.

Cu@rGO sheets were implanted in a PC matrix to prevent aggregation, and the resulting product was denoted as Cu@rGO-PC-*x*. Scheme 1 shows the preparation procedure of Cu@rGO-PC-*x*. As shown in Figure 2c−f, morphological observations of Cu@rGO-PC-*x* confirmed direct evidence of dispersing Cu@rGO sheets in the PC matrix. The edges of the rGO sheets in Cu@rGO-PC-25 showed a clear outline and could easily be discerned (Figure 2c). By comparison, neat PC (Figure 2f) had a smooth surface, and no sheet-like structure could be found in the region. Benefiting from the dispersion of Cu@rGO sheets in the PC matrix, oxidation by Cu@rGO-PC-25 afforded 65.4% styrene conversion within 4 h; this conversion rate is considerably higher than that of Cu@rGO (bulk). Cu@rGO-PC-25 exhibited lower activity compared with Cu@rGO (powder). Considering the catalytic activities of PC and rGO, differences in styrene conversion between Cu@rGO-PC-25 and Cu@rGO (powder) may be primarily attributed to differences in the nanostructures of catalysts. In particular, as shown in Scheme 1, certain copper species anchored on the rGO sheets are wrapped in the PC matrix in Cu@rGO-PC-25. With an increase in the percentage of PC in samples, the outline of rGO sheets became blurred (Figure 2d,e). The Cu@rGO sheets in Cu@rGO-PC-75 were nearly completely wrapped by the PC matrix (Figure 2e). Thus, we speculated that styrene conversion would decrease with an increase in the PC percentage in the corresponding samples. To confirm this prediction, we evaluated the catalytic activities of Cu@rGO-PC-50 and Cu@rGO-PC-75 for styrene oxidation. Under identical reaction conditions, the catalytic activities of these samples (Table 1, entries 4 and 5) were clearly inferior to that of Cu@rGO-PC-25. Among the Cu@rGO-PC-*x* samples tested, Cu@rGO-PC-75 exhibited the lowest activity; however, the activity of this sample remained higher than that of PC. This result suggests that a large amount of the Cu NPs is wrapped by the PC matrix, consistent with the results illustrated in SEM images. Therefore, increasing the percentage of PC in Cu@rGO-PC-*x* may reasonably be concluded to have an adverse impact on styrene conversion. When PC or rGO was employed as the catalyst, benzaldehyde was the primary product of styrene oxidation. Benzaldehyde and styrene oxide were the major products formed in the presence of copper species. Considering these results, copper species may be concluded to be primarily responsible for the catalytic activity of Cu@rGO-PC-*x* even in the presence of PC and rGO.

The nanostructure of Cu@rGO-PC-*x* reflected two types of Cu NPs in samples (Scheme 1). Certain Cu NPs anchored onto the surface of the rGO sheets are exposed to reactive species and could be responsible for the catalytic activity; these particles may be denoted as active Cu NPs. Alternatively, certain Cu NPs are wrapped in the composite matrix, which renders them inaccessible to reactant molecules; these particles are denoted as inactive Cu NPs. Leaching of copper from the catalysts may be primarily attributed to the oxidation of active Cu NPs by TBHP during the reaction; however, copper

https://doi.org/10.1021/acsomega.1c02031
ACS Omega 2021, 6, 18157−18168

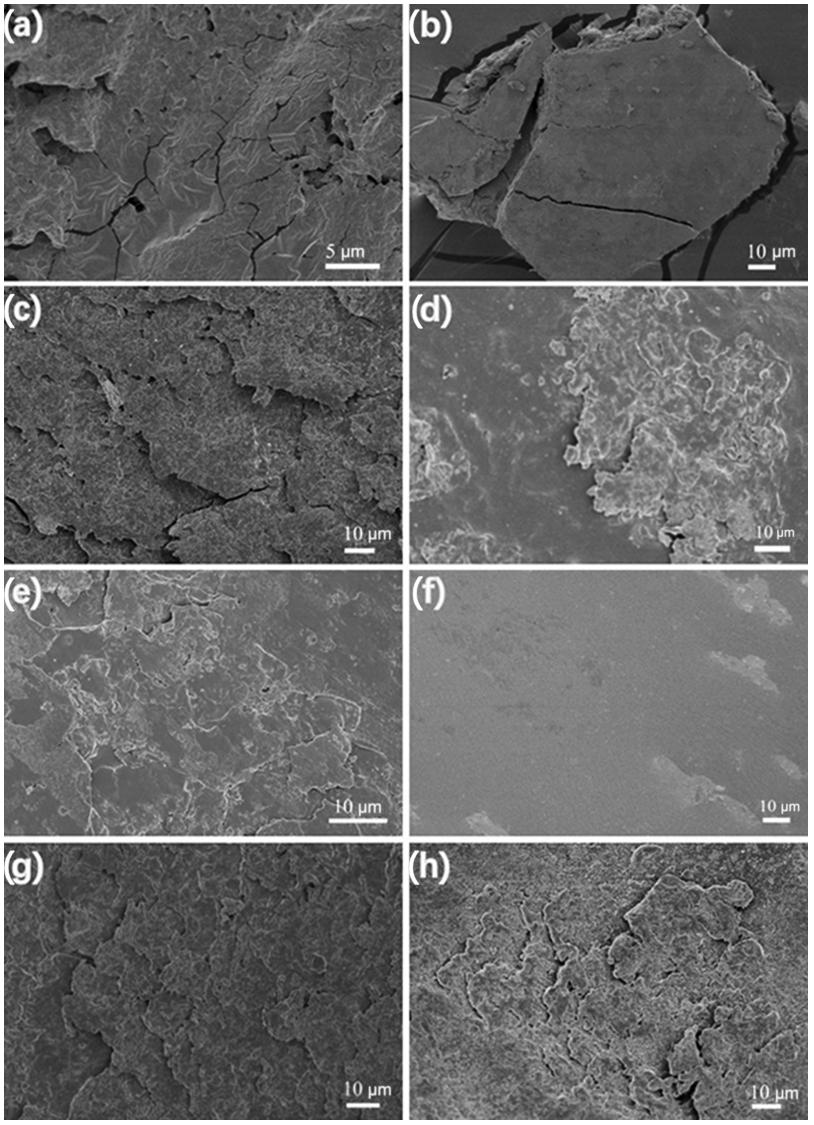

Figure 2. SEM images of (a) Cu@rGO (powder), (b) Cu@rGO (bulk), (c) Cu@rGO-PC-25, (d) Cu@rGO-PC-50, (e) Cu@rGO-PC-75, (f) PC, (g) CuO@rGO-PC, and (h) CuO@rGO-PC-R.

species in the composite matrix of Cu@rGO-PC-*x* cannot contribute to the generation of free copper ions. The reactant mixtures were analyzed by ICP-MS after removing the catalysts; Table 2 presents the results. The amount of copper species in the filtrate when Cu@rGO-PC-25 was used as the catalyst was 68.90 ppm, which is less than that obtained when Cu@rGO (powder) was used. This result shows that the amount of active Cu NPs in Cu@rGO (powder) is larger than that in Cu@rGO-PC-25, once again confirming the nanostructure of Cu@rGO-PC-*x* depicted in Scheme 1. The amount of copper in the filtrate leached from Cu@rGO (bulk) was 55.70 ppm, thus suggesting that the overall ranking of the amount of active Cu NPs in the samples is as follows: Cu@rGO (powder) > Cu@rGO-PC-25 > Cu@rGO (bulk). Based on this order, Cu@rGO (bulk) may be expected to show inferior activity compared with Cu@rGO (powder) and Cu@rGO-PC-25, which is in good agreement with the above-mentioned results (Table 1; entries 3, 6, and 7). Thus, the catalytic activities of the obtained products are clearly positively correlated with the amount of active Cu NPs they contain.

2.2. Catalytic Performance of CuO@rGO-PC. X-ray photoelectron spectroscopy (XPS) measurements were performed to explain the chemical compositions and valence states of Cu@rGO-PC-25 and CuO@rGO-PC (Figure 4). In Figure 4c, the binding energies at ∼931.8 and 951.0 eV confirmed the presence of Cu(0) species in Cu@rGO-PC-25.[57,58] The Cu 2p XPS spectrum of CuO@rGO-PC demonstrated two peaks of Cu $2p_{3/2}$ at 933.0 eV and Cu $2p_{1/2}$ at 952.6 eV, which correspond to Cu(II) species.[59] Because of the strong interactions of CuO NPs with the graphene sheet surfaces via covalent bonding, the binding energies of Cu $2p_{3/2}$ and Cu $2p_{1/2}$ are lower compared with the values previously reported for CuO.[60−62] This result indicates that copper oxides formed on the surface of Cu NPs after the initial reaction of Cu@rGO-PC-25 because of the oxidation brought about by TBHP. The SEM elemental mapping of CuO@rGO-PC (Figure 5) indicates that copper species are homogeneously distributed throughout the CuO_x@rGO sheets outside the PC matrix. Thus, CuO may be responsible for the catalytic activity of CuO@rGO-PC.

https://doi.org/10.1021/acsomega.1c02031
ACS Omega 2021, 6, 18157−18168

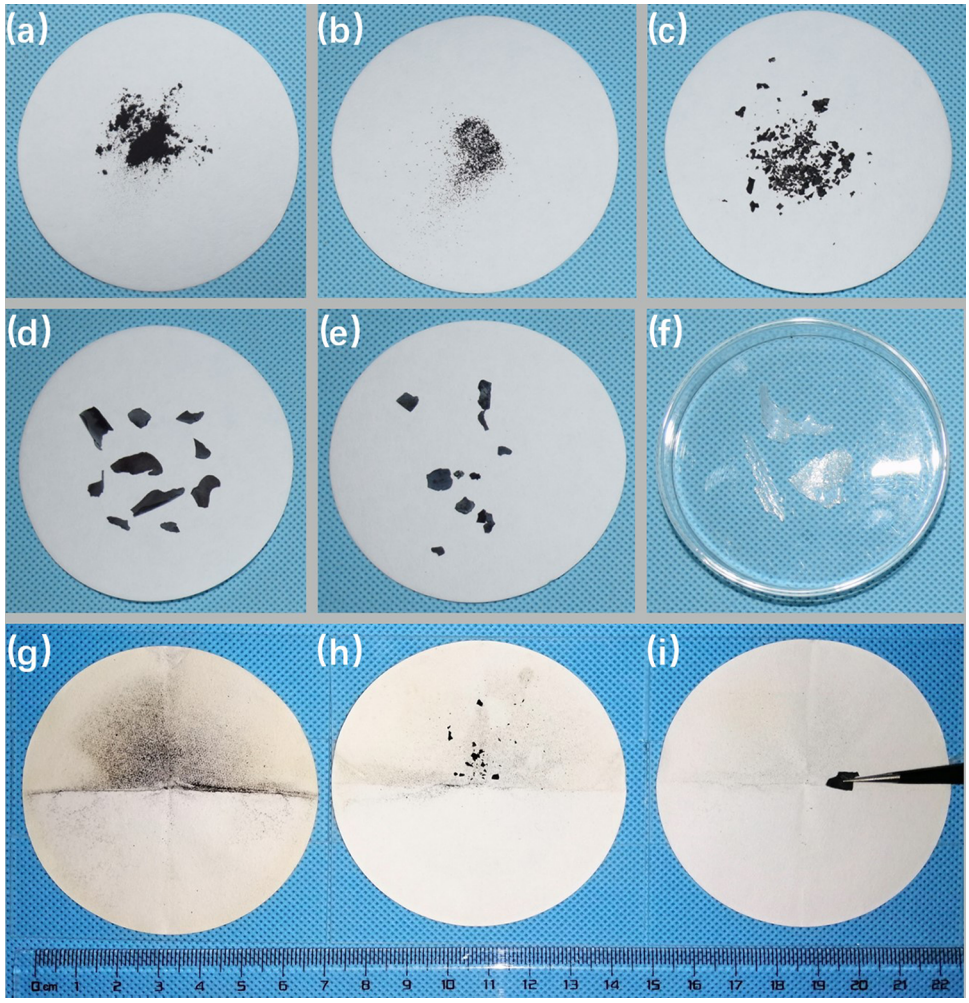

Figure 3. Optical images of (a) commercial CuO, (b) Cu@rGO (powder), (c) Cu@rGO (bulk), (d) Cu@rGO-PC-25, (e) CuO@rGO-PC, and (f) PC. Commercial CuO and Cu@rGO (powder) are powder catalysts, while Cu@rGO-PC-25, CuO@rGO-PC, and PC are self-supported thin films. Recovery of (g) Cu@rGO (powder), (h) Cu@rGO (bulk), and (i) CuO@rGO-PC. CuO@rGO-PC was recovered by tweezers and the reaction of the mixture was filtrated, while Cu@rGO (powder) and Cu@rGO (bulk) were recovered by filtration.

Scheme 1. Schematic Illustration of the Synthetic Process of Cu@rGO-PC-*x* and CuO@rGO-PC

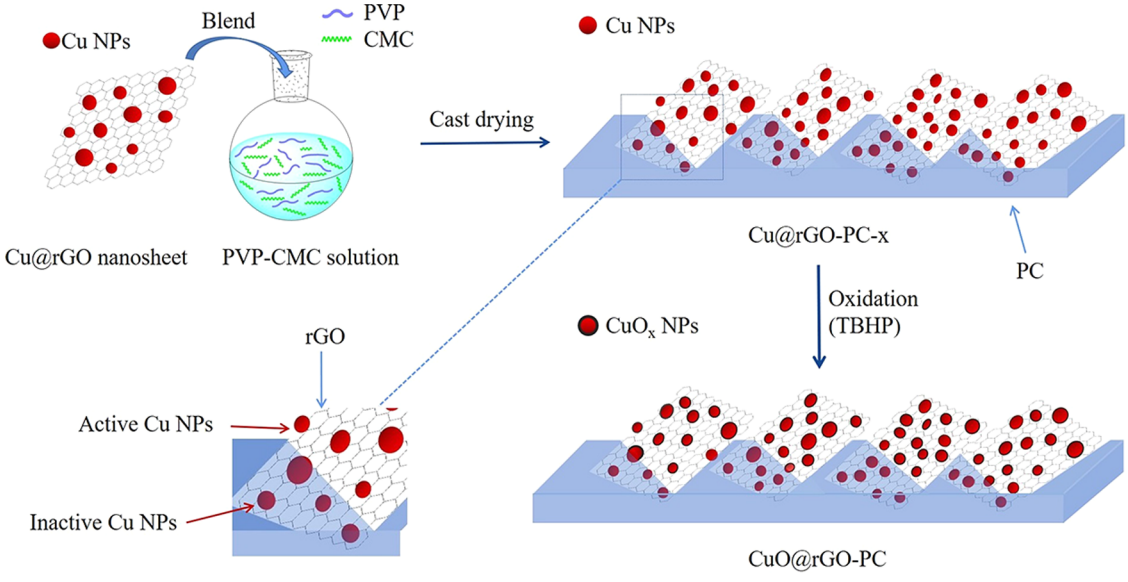

https://doi.org/10.1021/acsomega.1c02031
ACS Omega 2021, 6, 18157−18168

Table 2. Comparison of the Amounts of Copper Leaching with Different Copper-Based Catalysts

		amount of Cu leached	
entry	catalyst	[ppm][a]	[%][b]
1	Cu@rGO (powder)	85.36	22.5
2	Cu@rGO (bulk)	55.70	14.7
3	Cu@rGO-PC-25	68.90	18.1
4	commercial CuO	1.78	0.5
5	CuO@rGO-PC	0.88	0.2

[a]Determined by ICP-MS. [b]Percentages refer to the total amount of Cu content in the corresponding catalysts.

The structure of commercial CuO was investigated by XRD. As shown in Figure 6e, the peaks corresponding to the 110, 002, 111, $\bar{2}02$, $\bar{3}11$, and 220 planes are derived from the standard CuO phase (JCPDS 80-1917).[63] No indication for the presence of cuprous oxides and pure copper is visible, suggesting the high purity of the commercial CuO. Oxidation by commercial CuO afforded 49.3% styrene conversion and 83.7% selectivity for the primary products under the present conditions. Compared with commercial CuO, CuO@rGO-PC had much higher catalytic activity, with a styrene conversion rate of 64.6% (Table 1, entry 2). Moreover, we compared the catalytic activity of CuO@rGO-PC with that of Cu@rGO-PC-25 for styrene oxidation and investigated the effect of reaction time on the catalytic performance of Cu@rGO-PC-25 and CuO@rGO-PC. As shown in Figure 6a, the conversion of styrene over Cu@rGO-PC-25 steadily increased, and 88.0% conversion was achieved when the reaction time was increased to 6 h. The catalytic behavior of CuO@rGO-PC was similar to that of Cu@rGO-PC-25; however, the conversion of styrene over the former, at 64.6% within 4 h and 87.0% within 6 h, was slightly lower than that over the latter. The selectivities of CuO@rGO-PC for styrene oxide and benzaldehyde (Figure 6c) were comparable with those of Cu@rGO-PC-25 (Figure 6b). We can thus conclude that the catalytic activity of CuO@rGO-PC for the liquid-phase oxidation of styrene is comparable with that of Cu@rGO-PC-25 under identical conditions. As reported earlier, the amount of copper leached when Cu@rGO-PC-25 was used as the catalyst was 68.90 ppm; by comparison, only trace amounts of copper (0.88 ppm) were detected when CuO@rGO-PC was tested. Because copper ion was also active for this reaction (Table 1, entry 8), CuO@rGO-PC was selected for further study via recycling tests.

2.3. Robustness of CuO@rGO-PC. Both isotropic and oriented Cu NPs anchored on graphene have been used as catalytic films for the nucleophilic addition of anilines to form guanidines.[64] Generally, these films are supported on a quartz plate by spin coating and tested in a sealed reinforced glass reactor with the reaction mixture. However, the as-synthesized Cu@rGO-PC-*x* series catalysts are self-supported films (inset, Figure 6a) that could be cut into small pieces and directly added to the reaction mixture (Figure 3d). As shown in Figure 2g, CuO@rGO-PC maintained a microstructural framework similar to that of Cu@rGO-PC-25 (Figure 2c); this result reveals that Cu@rGO-PC-25 does not undergo major microstructural changes during the oxidation of styrene. The macrostructural stability of the CuO@rGO-PC in acetonitrile was directly evaluated by observing the integrity of the material after the reaction. The optical images shown in Figure 3e,i indicate that CuO@rGO-PC could be easily recovered by

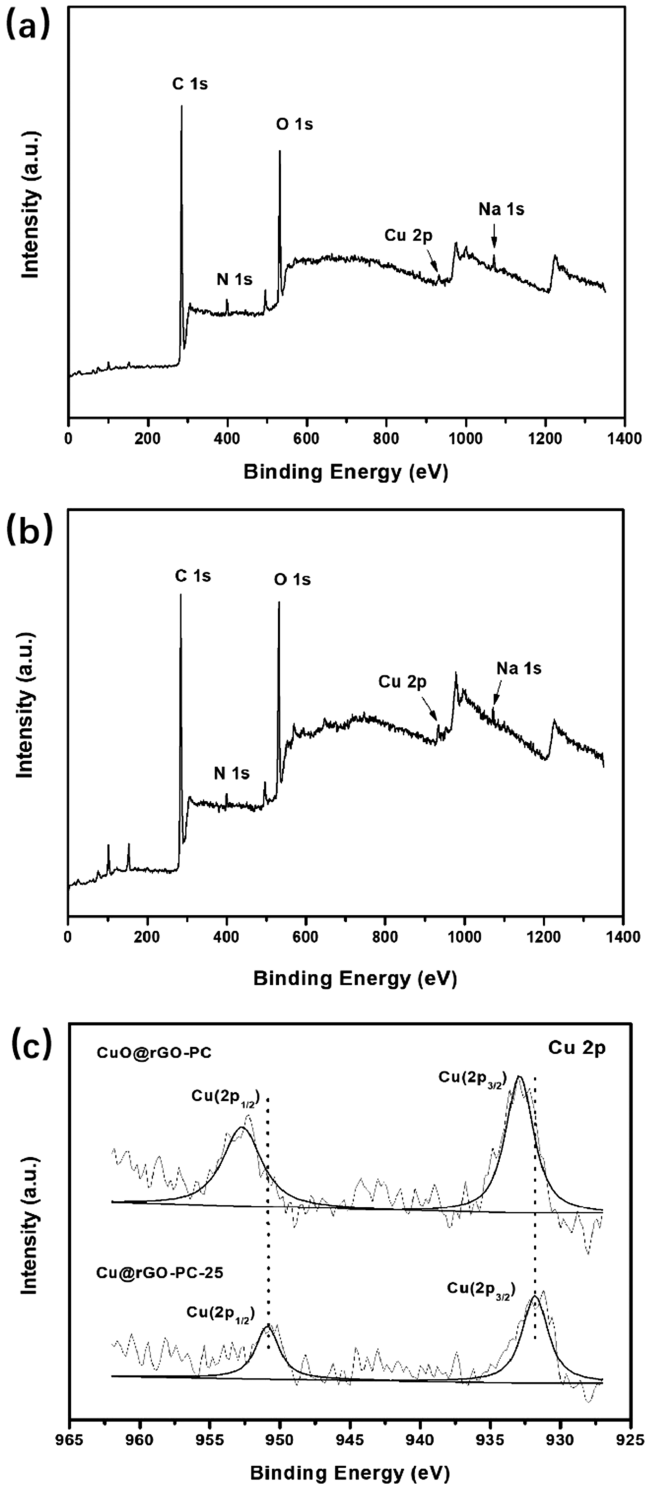

Figure 4. XPS survey spectra of (a) Cu@rGO-PC-25 and (b) CuO@rGO-PC. Cu 2p XPS spectra of (c) Cu@rGO-PC-25 and CuO@rGO-PC.

tweezers, and its integrity was maintained as a macroscopically usable film during the reaction. This characteristic of CuO@rGO-PC is different from that of Cu@rGO (powder), which is difficult to separate and recover from the reaction mixture (Figure 3g). The recovered CuO@rGO-PC was washed with acetonitrile, dried under vacuum for 12 h, and then employed in subsequent reactions. Reusability studies with CuO@rGO-PC revealed ~4% loss in catalytic activity after five consecutive

https://doi.org/10.1021/acsomega.1c02031
ACS Omega 2021, 6, 18157−18168

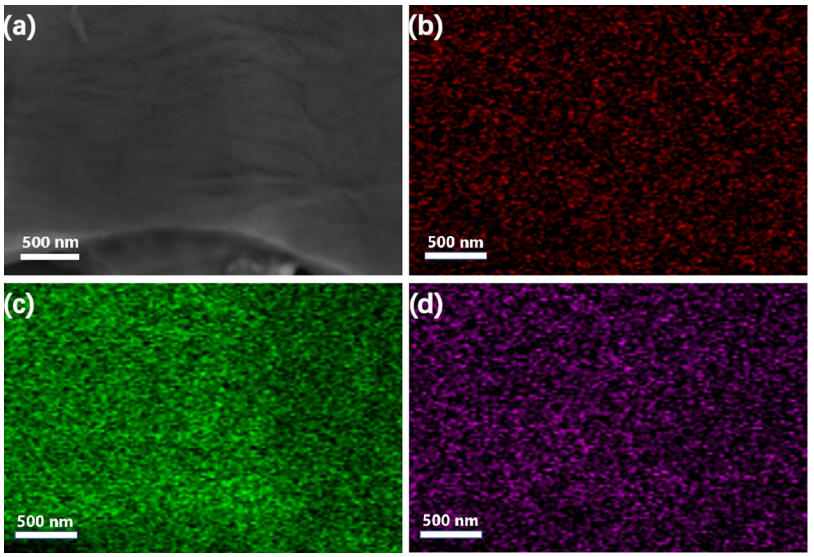

Figure 5. (a) SEM image of a CuO_x@rGO sheet in CuO@rGO-PC and relevant elemental mapping images of (b) copper, (c) carbon, and (d) oxygen in the selected region.

runs (Figure 6d). Moreover, slightly lower selectivity for styrene oxide and higher selectivity for benzaldehyde were observed. The primary microstructure of CuO@rGO-PC was preserved after the recycling test (Figure 2h). The FT-IR spectra of CuO@rGO-PC and CuO@rGO-PC-R illustrated in Figure 6f demonstrated vibration bands attributable to −OH (3352 cm^{-1}), $-CH_2$ (2929 cm^{-1}), C═O (1654 cm^{-1}), COO− (1368 cm^{-1}), C−H (1320 cm^{-1}), and C−O (1108 cm^{-1}) groups.[65−68] The strong and broad peak at 1654 cm^{-1} could be assigned to the stretching vibration of C═O in PVP rings.[65] The absorption peak at 2929 cm^{-1} confirms the presence of asymmetric CH_2, and the peak at 822 cm^{-1} represents the characteristic vibrations of PVP rings.[66] The peaks at 1368 cm^{-1} (COO− symmetric stretching vibrations), 1320 cm^{-1} (C−H bending vibrations), and 1108 cm^{-1} (C−O stretching vibrations) belong to CMC.[67,68] These FT-IR results indicate the presence of PVP and CMC in the tested samples.

CuO@rGO-PC, CuO@rGO-PC-R, rGO, and PC were evaluated by TGA. As shown in Figure 7a, all of the samples reveal a weight loss at ∼100 °C, which may be attributed to the evaporation of absorbed water molecules. The TGA curve of PC (Figure 7a,c) showed a rapid weight loss of 67.7% at temperatures of <540 °C corresponding to the decomposition of CMC and PVP.[69] PC showed weight loss between 220 and 320 °C, which is related to the degradation of CMC, and between 320 and 540 °C, which could be attributed to the degradation of PVP. CuO@rGO-PC and CuO@rGO-PC-R exhibited superior thermal stability compared with PC in a N_2 atmosphere at 1000 °C. This result could be attributed to the effect of the CuO_x@rGO sheets on the mechanical and thermal properties of the resultant films.[70] The TGA profiles of CuO@rGO-PC and CuO@rGO-PC-R shown in Figure 7a,b exhibit similar weight loss plots between 160 and 540 °C, which could be attributed to the degradation of PVP and CMC. Both PVP and CMC make up ∼38.5% of the total weight of CuO@rGO-PC; however, 43.9% weight loss could be observed in the TGA plot of CuO@rGO-PC-R from 160 to 540 °C. The discrepancy in weight loss may be attributed to the leaching of CuO_x@rGO in CuO@rGO-PC during the styrene oxidation. Such leaching may explain the loss of catalytic activity of CuO@rGO-PC observed in the reusability studies (Figure 6d).

3. CONCLUSIONS

In this work, we successfully developed a facile and controllable strategy to fabricate self-supported catalytic films. The XPS, TEM, and SEM results revealed that the films are composed of copper species anchored on the surface of rGO sheets incorporated in the PC matrix. Owing to the thorough dispersion of CuO_x@rGO sheets, CuO@rGO-PC demonstrated excellent performance for styrene oxidation and afforded good selectivity for styrene oxide and benzaldehyde. Leaching studies demonstrated the truly heterogeneous nature of CuO@rGO-PC. In the absence of an inert substrate, CuO@rGO-PC could be recycled five times without any significant loss in its catalytic activity. After its reaction, CuO@rGO-PC could be conveniently removed from the reaction mixture by tweezers. Experimental investigations on the morphology and chemical components of the catalyst materials confirmed the robust nature of CuO@rGO-PC.

4. EXPERIMENTAL SECTION

4.1. General Considerations. All of the chemicals employed in the experiments were of analytical grade, purchased from HEOWNS Reagents Company, and used as received without further purification. Graphene oxide was directly used as received from XFNANO Materials Tech Co., Ltd.

4.2. Material Characterization. Transmission electron microscopy (TEM) was conducted using a high-resolution transmission electron microscope (Hitachi, HT7700) operated at 80.0 kV. All samples were dispersed in absolute ethanol solution by ultrasonication and then dropped onto a Cu grid. Surface morphologies were observed under a control scanning probe microscope (SEM, Hitachi, SU8010). SEM-energy dispersive spectroscopy (SEM-EDS) measurements were recorded using a ZEISS Gemini 300. X-ray photoelectron spectroscopy (XPS) measurements were performed using a PHI 5000 VersaProbe apparatus. Inductively coupled plasma-

https://doi.org/10.1021/acsomega.1c02031
ACS Omega 2021, 6, 18157−18168

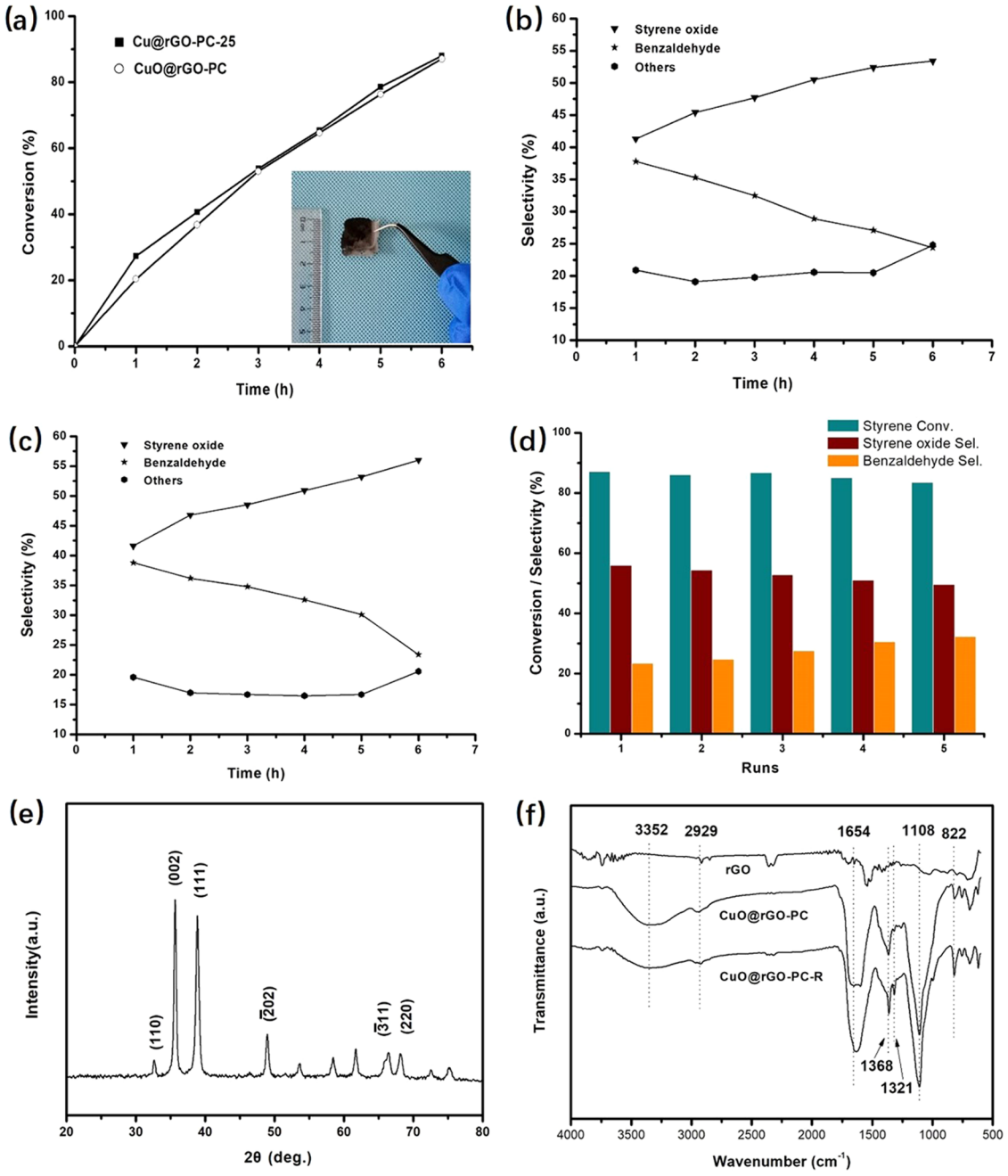

Figure 6. (a) Effect of reaction time on conversion of styrene oxidation catalyzed by Cu@rGO-PC-25 and CuO@rGO-PC. Inset: optical image of as-synthesized Cu@rGO-PC-25. (b) Effect of reaction time on the selectivity of styrene oxidation catalyzed by Cu@rGO-PC-25. (c) Effect of reaction time on the selectivity of styrene oxidation catalyzed by CuO@rGO-PC. Reaction conditions (a−c): styrene (2.0 mmol), catalyst (1.5 mol % Cu), CH_3CN (5 mL), *tert*-BuOOH (2 equiv), 70 °C. (d) Reusability of CuO@rGO-PC in styrene oxidation. Reaction conditions: styrene (2.0 mmol), catalyst (1.5 mol % Cu), CH_3CN (5 mL), *tert*-BuOOH (2 equiv), 70 °C, 6 h. (e) Powder XRD patterns of commercial CuO. (f) The FT-IR spectra of rGO, CuO@rGO-PC, and CuO@rGO-PC-R.

mass spectroscopy (ICP-MS) analysis was conducted using a Thermo iCAP6300 instrument to assess the copper concentrations in catalysts. The X-ray diffraction (XRD) patterns of the samples were recorded on a Rigaku Ultima IV diffractometer over the 2θ range of 20−80° using Cu Kα radiation at 40 kV and 40 mA. TGA (LECO TGA701) was performed in a N_2 atmosphere from 30 to 1000 °C at a heating rate of 10 °C/min. FTIR spectroscopy was conducted on a Shimadzu IRAffinity-1S spectrometer over the range of 600−4000 cm^{-1}.

4.3. Catalyst Preparation. *4.3.1. Preparation of Cu@rGO and rGO.* Cu NPs were located on GO through a solvothermal method, using $Cu(NO_3)_2{\cdot}3H_2O$ as a precursor. First, 100 mg of GO was dispersed in 100 mL of EG with vigorous stirring and sonication. Then, 1.7 mmol of $Cu(NO_3)_2{\cdot}3H_2O$ was dissolved into 50 mL of PVP-EG solution (16 mg/mL) in a three-neck round-bottom flask. Subsequently, the solution was added dropwise into the GO-EG suspension and continuously stirred for 1 h at room temperature. A certain amount of 1 M KOH solution was then added to the abovementioned mixture to adjust the pH to ∼10. Finally, under constant stirring, the

https://doi.org/10.1021/acsomega.1c02031
ACS Omega 2021, 6, 18157−18168

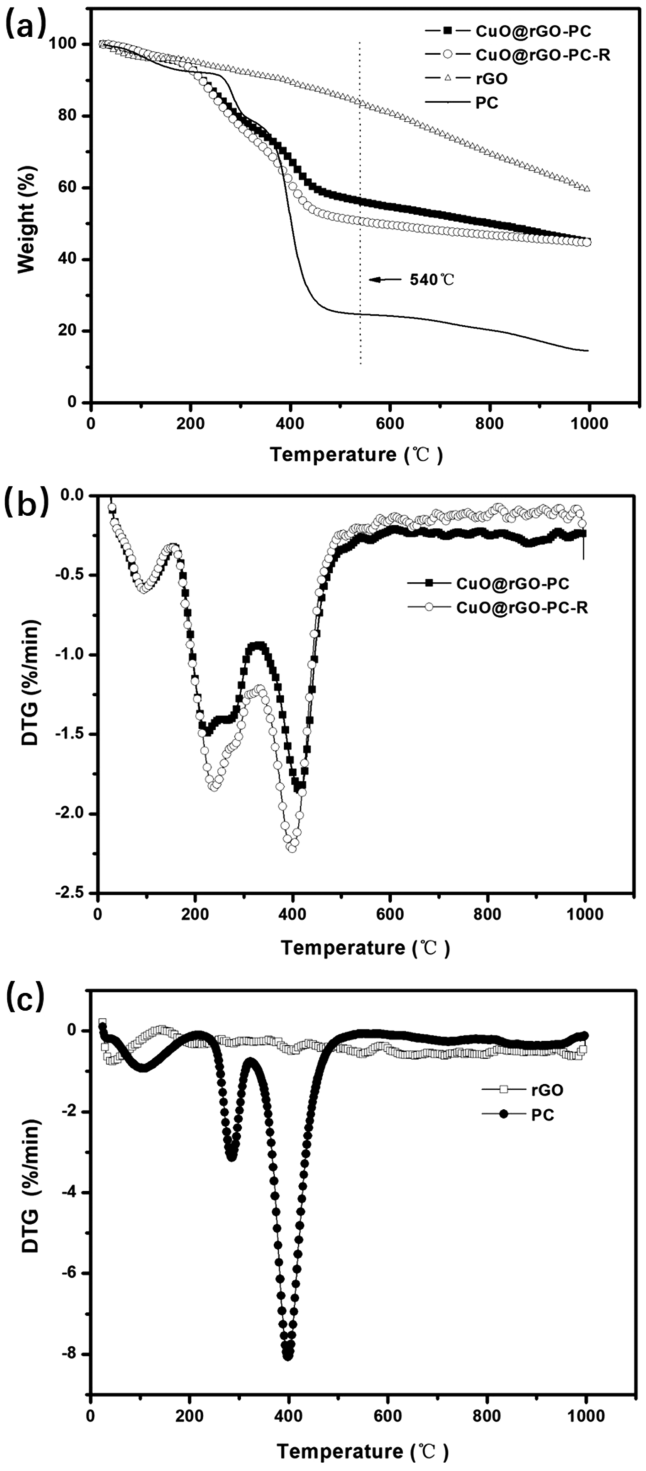

Figure 7. (a) TG curves of PC, rGO, CuO@rGO-PC, and CuO@rGO-PC-R. DTG curves of (b) CuO@rGO-PC and CuO@rGO-PC-R and (c) PC and rGO.

flask was placed in an oil bath at 150 °C for 2 h. After cooling to room temperature, products were separated by centrifugation (10 000 rpm, 10 min) and washed three times with deionized water and ethanol in sequence. The dark brown slurry was dried in vacuum at 80 °C for 12 h. The obtained solid was denoted as Cu@rGO. The as-synthesized Cu@rGO powders were separated from flakes by sieving and denoted as Cu@rGO (powder) and Cu@rGO (bulk). The weight ratio of Cu@rGO (powder)/Cu@rGO (bulk) was 10.3:100. For comparison, the same procedure was used to prepare rGO without $Cu(NO_3)_2{\cdot}3H_2O$.

4.3.2. Preparation of Cu@rGO-PC-x and PC. The wet dark brown slurry obtained in the previous section was redispersed in 20 mL of ethanol with vigorous stirring and sonication and denoted as Cu@rGO-ethanol suspension. Then, 200 mg of CMC was dissolved into 100 mL of PVP solution (2 mg/mL) and stirred for 30 min. Different volumes of the PVP-CMC solution (0−100 mL) were added dropwise to the Cu@rGO-ethanol suspension with continuous stirring for 2 h at room temperature. The mixture obtained was cast into a porcelain crucible and then coagulated in an oven at 120 °C for 3 h. The black product was further dried under an IR lamp for 1 h. The resultant films were denoted as Cu@rGO-PC-*x*, where *x* represents the added volume of the PVP-CMC solution. For comparison, PC was synthesized using the same procedure but without the Cu@rGO-ethanol suspension.

4.3.3. Preparation of CuO@rGO-PC. The Cu@rGO-PC-25 recovered after styrene oxidation for 6 h (Section 4.4.1) was denoted as CuO@rGO-PC.

4.4. Catalytic Performance Evaluation. *4.4.1. Styrene Oxidation.* Prior to the catalytic test, the films were scrapped off from the porcelain crucible and cut into small pieces. In a typical reaction, 2.0 mmol of styrene, TBHP (2 equiv; 70% aqueous solution), catalysts in the required amounts, and 5 mL of acetonitrile were placed in a round-bottom flask with a reflux condenser. The flask containing the reaction mixture was immersed in a silicone oil bath preheated to 70 °C, and the mixture was refluxed for the required time under atmosphere and then cooled to room temperature. The catalyst was then removed by filtration or tweezers. The products were analyzed by gas chromatography (GC) with a capillary column (poly(ethylene glycol), 30 m × 0.53 mm × 0.50 μm).

4.4.2. Reuse Experiments. The reactions were performed as indicated in the previous section. The CuO@rGO-PC catalyst was removed by tweezers after each reaction, and the liquid phase was filtered before GC analysis. The CuO@rGO-PC catalyst was exhaustively washed with acetonitrile and dried under vacuum for 12 h. After the fifth run, the sample was recovered and denoted as CuO@rGO-PC-R.

AUTHOR INFORMATION

Corresponding Author

Bin Du − *School of Chemistry, Tiangong University, Tianjin 300387, China;* orcid.org/0000-0003-3763-8879; Email: dbin@tiangong.edu.cn

Authors

Lili Qiu − *School of Chemistry, Tiangong University, Tianjin 300387, China*

Yuting Chen − *School of Chemistry, Tiangong University, Tianjin 300387, China*

Ziqi Zhang − *School of Chemistry, Tiangong University, Tianjin 300387, China*

Complete contact information is available at: https://pubs.acs.org/10.1021/acsomega.1c02031

Notes

The authors declare no competing financial interest.

https://doi.org/10.1021/acsomega.1c02031
ACS Omega 2021, 6, 18157−18168

■ ACKNOWLEDGMENTS

The authors would like to thank Tianjin Institute of Industrial Biotechnology, Chinese Academy of Sciences, for the support of SEM and TEM test.

■ REFERENCES

(1) Novoselov, K. S.; Geim, A. K.; Morozov, S. V.; Jiang, D.; Zhang, Y.; Dubonos, S. V.; Grigorieva, I. V.; Firsob, A. A. Electric Field Effect in Atomically Thin Carbon Films. *Science* **2004**, *306*, 666−669.

(2) Ohta, T.; Bostwick, A.; Seyller, T.; Horn, K.; Rotenberg, E. Controlling the Electronic Structure of Bilayer Graphene. *Science* **2006**, *313*, 951−954.

(3) Gerber, I. C.; Serp, P. A Theory/Experience Description of Support Effects in Carbon Supported Catalysts. *Chem. Rev.* **2020**, *120*, 1250−1349.

(4) de Almeida, L. D.; Wang, H.; Junge, K.; Cui, X.; Beller, M. Recent Advances in Catalytic Hydrosilylations: Developments Beyond Traditional Platinum Catalysts. *Angew. Chem., Int. Ed.* **2021**, *60*, 550−565.

(5) Navalon, S.; Dhakshinamoorthy, A.; Alvaro, M.; Garcia, H. Metal nanoparticles supported on two-dimensional graphenes as heterogeneous catalysts. *Coord. Chem. Rev.* **2016**, *312*, 99−148.

(6) Wang, Y.; Mao, J.; Meng, X.; Yu, L.; Deng, D.; Bao, X. Catalysis with Two-Dimensional Materials Confining Single Atoms: Concept, Design, and Applications. *Chem. Rev.* **2019**, *119*, 1806−1854.

(7) Kim, K. S.; Zhao, Y.; Jang, H.; Lee, S. Y.; Kim, J. M.; Kim, K. S.; Ahn, J. H.; Kim, P.; Choi, J. Y.; Hong, B. H. Large-Scale Pattern Growth of Graphene Films for Stretchable Transparent Electrodes. *Nature* **2009**, *457*, 706−710.

(8) Rasool, H. I.; Song, E. B.; Mecklenburg, M.; Regan, B. C.; Wang, K. L.; Weiller, B. H.; Gimzewski, J. K. Atomic-Scale Characterization of Graphene Grown on Copper (100) Single Crystals. *J. Am. Chem. Soc.* **2011**, *133*, 12536−12543.

(9) Aprojanz, J.; Rosenzweig, P.; Nhung Nguyen, T. T.; Karakachian, H.; Küster, K.; Starke, U.; Lukosius, M.; Lippert, G.; Sinterhauf, A.; Wenderoth, M.; Zakharov, A. A.; Tegenkamp, C. High-Mobility Epitaxial Graphene on Ge/Si (100) Substrates. *ACS Appl. Mater. Interfaces* **2020**, *12*, 43065−43072.

(10) Wang, Z. J.; Dong, J.; Li, L.; Dong, G.; Cui, Y.; Yang, Y.; Wei, W.; Blume, R.; Li, Q.; Wang, L.; Xu, X.; Liu, K.; Barroo, C.; Frenken, J. W. M.; Fu, Q.; Bao, X.; Schlogl, R.; Ding, F.; Willinger, M. G. The Coalescence Behavior of Two- Dimensional Materials Revealed by Multiscale *In Situ* Imaging During Chemical Vapor Deposition Growth. *ACS Nano* **2020**, *14*, 1902−1918.

(11) Novotny, Z.; Nguyen, M.-T.; Netzer, F. P.; Glezakou, V.-A.; Rousseau, R.; Dohnalek, Z. Formation of supported graphene oxide: Evidence for enolate species. *J. Am. Chem. Soc.* **2018**, *140*, 5102−5109.

(12) Zhu, Y.; James, D. K.; Tour, J. M. New Routes to Graphene, Graphene Oxide and Their Related Applications. *Adv. Mater.* **2012**, *24*, 4924−4955.

(13) Fan, X.; Yuan, W.; Zhang, D. H.; Li, C. M. Heteropolyacid-Mediated Self-Assembly of Heteropolyacid-Modified Pristine Graphene Supported Pd Nanoflowers for Superior Catalytic Performance toward Formic Acid Oxidation. *ACS Appl. Energy Mater.* **2018**, *1*, 411−420.

(14) Li, L.; Wu, Y.; Lu, J.; Nan, C.; Li, Y. Synthesis of Pt−Ni/graphene via in situ reduction and its enhanced catalyst activity for methanol oxidation. *Chem. Commun.* **2013**, *49*, 7486−7488.

(15) Tran, T. P. N.; Thakur, A.; Trinh, D. X.; Dao, A. T. N.; Taniike, T. Design of Pd@Graphene Oxide Framework Nanocatalyst with Improved Activity and Recyclability in Suzuki-Miyaura Cross-Coupling Reaction. *Appl. Catal., A* **2018**, *549*, 60−67.

(16) Carneiro, J. F.; Paulo, M. J.; Siaj, M.; Tavares, A. C.; Lanza, M. R. V. Nb_2O_5 nanoparticles supported on reduced graphene oxide sheets as electrocatalyst for the H_2O_2 electrogeneration. *J. Catal.* **2015**, *332*, 51−61.

(17) Son, S.; Cho, Y.; Hong, H.-K.; Lee, J.; Kim, J. H.; Kim, K.; Lee, Y.; Yoon, A.; Shin, H.-J.; Lee, Z. Spontaneous Formation of a ZnO Monolayer by the Redox Reaction of Zn on Graphene Oxide. *ACS Appl. Mater. Interfaces* **2020**, *12*, 54222−54229.

(18) Gao, W.; Alemany, L. B.; Ci, L.; Ajayan, P. M. New insights into the structure and reduction of graphite oxide. *Nat. Chem.* **2009**, *1*, 403−408.

(19) Gong, X.; Liu, G.; Li, Y.; Yu, D. Y. W.; Teoh, W. Y. Functionalized-Graphene Composites: Fabrication and Applications in Sustainable Energy and Environment. *Chem. Mater.* **2016**, *28*, 8082−8118.

(20) Hu, M.; Yao, Z.; Wang, X. Graphene-Based Nanomaterials for Catalysis. *Ind. Eng. Chem. Res.* **2017**, *56*, 3477−3502.

(21) Pomerantseva, E.; Bonaccorso, F.; Feng, X.; Cui, Y.; Gogotsi, Y. Energy storage: The future enabled by nanomaterials. *Science* **2019**, *366*, No. eaan8285.

(22) Machado, B. F.; Serp, P. Graphene-based materials for catalysis. *Catal. Sci. Technol.* **2012**, *2*, 54−75.

(23) Men, B.; Sun, Y.; Tang, Y.; Zhang, L.; Chen, Y.; Wan, P.; Pan, J. Highly Dispersed Ag-Functionalized Graphene Electrocatalyst for Oxygen Reduction Reaction in Energy-Saving Electrolysis of Sodium Carbonate. *Ind. Eng. Chem. Res.* **2015**, *54*, 7415−7422.

(24) Rostamnia, S.; Doustkhah, E.; Karimi, Z.; Amini, S.; Luque, R. Surfactant-Exfoliated Highly Dispersive Pd-Supported Graphene Oxide Nanocomposite as a Catalyst for Aerobic Aqueous Oxidations of Alcohols. *ChemCatChem* **2015**, *7*, 1678−1683.

(25) Wang, J. C.; Kondrat, S. A.; Wang, Y. Y.; Brett, G. L.; Giles, C.; Bartley, J. K.; Lu, L.; Liu, Q.; Kiely, C. J.; Hutchings, G. J. Au-Pd Nanoparticles Dispersed on Composite Titania/Graphene Oxide Supports as a Highly Active Oxidation Catalyst. *ACS Catal.* **2015**, *5*, 3575−3587.

(26) Li, R.; Yang, Y.; Wu, D.; Li, K.; Qin, Y.; Tao, Y.; Kong, Y. Covalent functionalization of reduced graphene oxide aerogels with polyaniline for high performance supercapacitors. *Chem. Commun.* **2019**, *55*, 1738−1741.

(27) Xia, Q.-H.; Ge, H.-Q.; Ye, C.-P.; Liu, Z.-M.; Su, K.-X. Advances in homogeneous and heterogeneous catalytic asymmetric epoxidation. *Chem. Rev.* **2005**, *105*, 1603−1662.

(28) Lane, B. S.; Burgess, K. Metal-Catalyzed Epoxidations of Alkenes with Hydrogen Peroxide. *Chem. Rev.* **2003**, *103*, 2457−2473.

(29) Grosso-Giordano, N. A.; Schroeder, C.; Okrut, A.; Solovyov, A.; Schottle, C.; Chasse, W.; Marinkovic, N.; Koller, H.; Zones, S. I.; Katz, A. Outer-Sphere Control of Catalysis on Surfaces: A Comparative Study of Ti (IV) Single-Sites Grafted on Amorphous versus Crystalline Silicates for Alkene Epoxidation. *J. Am. Chem. Soc.* **2018**, *140*, 4956−4960.

(30) Botubol-Ares, J. M.; Hanson, J. R.; Hernández-Galán, R.; Collado, I. G. Mild Epoxidation of Allylic Alcohols Catalyzed by Titanium (III) Complexes: Selectivity and Mechanism. *ACS Omega* **2017**, *2*, 3083−3090.

(31) Jiang, J.; Chen, H.-Y.; Zhou, X.-T.; Chen, Y.-J.; Xue, C.; Ji, H.-B. Biomimetic Aerobic Epoxidation of Alkenes Catalyzed by Cobalt Porphyrin under Ambient Conditions in the Presence of Sunflower Seeds Oil as a Co-Substrate. *ACS Omega* **2020**, *5*, 4890−4899.

(32) Tian, S.; Peng, C.; Dong, J.; Xu, Q.; Chen, Z.; Zhai, D.; Wang, Y.; Gu, L.; Hu, P.; Duan, H.; Wang, D.; Li, Y. High-Loading Single-Atomic-Site Silver Catalysts with an $Ag_1-C_2N_1$ Structure Showing Superior Performance for Epoxidation of Styrene. *ACS Catal.* **2021**, *11*, 4946−4954.

(33) Gawande, M. B.; Goswami, A.; Felpin, F. X.; Asefa, T.; Huang, X.; Silva, R.; Zou, X.; Zboril, R.; Varma, R. S. Cu and Cu-Based Nanoparticles: Synthesis and Applications in Catalysis. *Chem. Rev.* **2016**, *116*, 3722−3811.

(34) Ye, R. P.; Lin, L.; Wang, L. C.; Ding, D.; Zhou, Z.; Pan, P.; Xu, Z.; Liu, J.; Adidharma, H.; Radosz, M.; Fan, M.; Yao, Y. G. Perspectives on the active sites and catalyst design for the hydrogenation of dimethyl oxalate. *ACS Catal.* **2020**, *10*, 4465−4490.

(35) Torres, D.; Lopez, N.; Illas, F.; Lambert, R. M. Why Copper Is Intrinsically More Selective than Silver in Alkene Epoxidation:

https://doi.org/10.1021/acsomega.1c02031
ACS Omega 2021, 6, 18157−18168

Ethylene Oxidation on Cu (111) versus Ag (111). *J. Am. Chem. Soc.* **2005**, *127*, 10774−10775.
(36) Cropley, R. L.; Williams, F. J.; Urquhart, A. J.; Vaughan, O. P. H.; Tikhov, M. S.; Lambert, R. M. Efficient Epoxidation of a Terminal Alkene Containing Allylic Hydrogen Atoms: trans-Methylstyrene on Cu {111}. *J. Am. Chem. Soc.* **2005**, *127*, 6069−6076.
(37) Song, Y.-Y.; Dong, B.; Wang, S.-W.; Wang, Z.-R.; Zhang, M.; Tian, P.; Wang, G.-C.; Zhao, Z. Selective Oxidation of Propylene on Cu_2O (111) and Cu_2O (110) Surfaces: A Systematically DFT Study. *ACS Omega* **2020**, *5*, 6260−6269.
(38) Concepción, P.; Boronat, M.; García−García, S.; Fernández, E.; Corma, A. Enhanced Stability of Cu Clusters of Low Atomicity Against Oxidation. Effect on the Catalytic Redox Process. *ACS Catal.* **2017**, *7*, 3560−3568.
(39) Sonobe, K.; Tanabe, M.; Yamamoto, K. Enhanced Catalytic Performance of Subnano Copper Oxide Particles. *ACS Nano* **2020**, *14*, 1804−1810.
(40) Banerjee, D.; Jagadeesh, R. V.; Junge, K.; Pohl, M.-M.; Radnik, J.; Brckner, A.; Beller, M. Convenient and Mild Epoxidation of Alkenes Using Heterogeneous Cobalt Oxide Catalysts. *Angew. Chem., Int. Ed.* **2014**, *53*, 4359−4363.
(41) Trache, D.; Thakur, V. K.; Boukherroub, R. Cellulose Nanocrystals/Graphene Hybrids—A Promising New Class of Materials for Advanced Applications. *Nanomaterials* **2020**, *10*, 1523.
(42) Patniboon, T.; Hansen, H. A. N-Doped Graphene Supported on Metal-Iron Carbide as a Catalyst for the Oxygen Reduction Reaction: Density Functional Theory Study. *ChemSusChem* **2020**, *13*, 996−1005.
(43) Mao, X.; Zhang, L.; Kour, G.; Zhou, S.; Wang, S.; Yan, C.; Zhu, Z.; Du, A. Defective Graphene on the Transition-Metal Surface: Formation of Efficient Bifunctional Catalysts for Oxygen Evolution/Reduction Reactions in Alkaline Media. *ACS Appl. Mater. Interfaces* **2019**, *11*, 17410−17415.
(44) Huang, H.; Shi, H.; Das, P.; Qin, J.; Li, Y.; Wang, X.; Su, F.; Wen, P.; Li, S.; Lu, P.; Liu, F.; Li, Y.; Zhang, Y.; Wang, Y.; Wu, Z.-S.; Cheng, H.-M. The Chemistry and Promising Applications of Graphene and Porous Graphene Materials. *Adv. Funct. Mater.* **2020**, *30*, No. 1909035.
(45) Zhou, S.; Liu, N.; Wang, Z.; Zhao, J. Nitrogen-Doped Graphene on Transition Metal Substrates as Efficient Bifunctional Catalysts for Oxygen Reduction and Oxygen Evolution Reactions. *ACS Appl. Mater. Interfaces* **2017**, *9*, 22578−22587.
(46) Das, V. K.; Mazhar, S.; Gregor, L.; Stein, B. D.; Morgan, D. G.; Maciulis, N. A.; Pink, M.; Losovyj, Y.; Bronstein, L. M. Graphene Derivative in Magnetically Recoverable Catalyst Determines Catalytic Properties in Transfer Hydrogenation of Nitroarenes to Anilines with 2-Propanol. *ACS Appl. Mater. Interfaces* **2018**, *10*, 21356−21364.
(47) Jia, H.-P.; Dreyer, D. R.; Bielawski, C. W. C−H oxidation using graphite oxide. *Tetrahedron* **2011**, *67*, 4431−4464.
(48) Tang, P.; Hu, G.; Li, M.; Ma, D. Graphene-Based Metal-Free Catalysts for Catalytic Reactions in the Liquid Phase. *ACS Catal.* **2016**, *6*, 6948−6958.
(49) Primo, A.; Parvulescu, V.; Garcia, H. Graphenes as Metal-Free Catalysts with Engineered Active Sites. *J. Phys. Chem. Lett.* **2017**, *8*, 264−278.
(50) Wang, Y.; Xie, Y.; Sun, H.; Xiao, J.; Cao, H.; Wang, S. Efficient catalytic ozonation over reduced graphene oxide for p-hydroxylbenzoic acid (PHBA) destruction: Active site and mechanism. *ACS Appl. Mater. Interfaces* **2016**, *8*, 9710−9720.
(51) Wu, Q.; Zhu, M.; Cao, J.; Wang, X.; Liu, Y.; Xiang, C.; Shao, M.; Tian, H.; Kang, Z. Metal-free catalyst with large carbon defects for efficient directoverall water splitting in air at room pressure. *ACS Appl. Mater. Interfaces* **2020**, *12*, 30280−30288.
(52) Haas, I.; Shanmugam, S.; Gedanken, A. Pulsed Sonoelectrochemical Synthesis of Size-Controlled Copper Nanoparticles Stabilized by Poly(N-vinylpyrrolidone). *J. Phys. Chem. B* **2006**, *110*, 16947−16952.
(53) Feng, X.; Ma, H.; Huang, S.; Pan, W.; Zhang, X.; Tian, F.; Gao, C.; Cheng, Y.; Luo, J. Aqueous−Organic Phase-Transfer of Highly Stable Gold, Silver, and Platinum Nanoparticles and New Route for Fabrication of Gold Nanofilms at the Oil/Water Interface and on Solid Supports. *J. Phys. Chem. B* **2006**, *110*, 12311−12317.
(54) Sun, L.; Deng, Q.; Li, Y.; Deng, L.; Wang, Y.; Ren, X.; Zhang, P. Solvothermal synthesis of ternary Cu_2O-CuO-RGO composites as anode materials for high performance lithium-ion batteries. *Electrochim. Acta* **2016**, *222*, 1650−1659.
(55) Zhang, X.; Zhou, J.; Song, H.; Chen, X.; Fedoseeva, Y. V.; Okotrub, A. V.; Bulusheva, L. G. "Butterfly Effect" in CuO/Graphene Composite Nanosheets: a Small Interfacial Adjustment Triggers Big Changes in Electronic Structure and Li-Ion Storage Performance. *ACS Appl. Mater. Interfaces* **2014**, *6*, 17236−17244.
(56) Liu, W.; Zhang, J.; Bai, Z.; Jiang, G.; Li, M.; Feng, K.; Yang, L.; Ding, Y.; Yu, T.; Chen, Z.; Yu, A. Controllable Urchin-like $NiCo_2S_4$ Microsphere Synergized with Sulfur-doped Graphene as Bifunctional Catalyst for Superior Rechargeable Zn-Air Battery. *Adv. Funct. Mater.* **2018**, *28*, No. 1706675.
(57) Dutta, A.; Rahaman, M.; Mohos, M.; Zanetti, A.; Broekmann, P. Electrochemical CO_2 Conversion Using Skeleton (Sponge) Type of Cu Catalysts. *ACS Catal.* **2017**, *7*, 5431−5437.
(58) Zheng, X.; Zhang, Q.; Guo, Y.; Zhan, W.; Guo, Y.; Wang, Y.; Lu, G. Epoxidation of propylene by molecular oxygen over supported Ag−Cu bimetallic catalysts with low Ag loading. *J. Mol. Catal. A: Chem.* **2012**, *357*, 106−111.
(59) Gopiraman, M.; Deng, D.; Babu, S. G.; Hayashi, T.; Karvembu, R.; Kim, I. S. Sustainable and Versatile CuO/GNS Nanocatalyst for Highly Efficient Base Free Coupling Reactions. *ACS Sustainable Chem. Eng.* **2015**, *3*, 2478−2488.
(60) Janas, J.; Gurgul, J.; Socha, R. P.; Dzwigaj, S. Effect of Cu content on the catalytic activity of CuSiBEA zeolite in the SCR of NO by ethanol: Nature of the copper species. *Appl. Catal., B* **2009**, *91*, 217−224.
(61) Shafiei, M.; Hoshyargar, F.; Lipton-Duffin, J.; Piloto, C.; Motta, N.; O'Mullane, A. P. Conversion of n-Type CuTCNQ into p-Type Nitrogen-Doped CuO and the Implication for Room-Temperature Gas Sensing. *J. Phys. Chem. C* **2015**, *119*, 22208−22216.
(62) Durando, M.; Morrish, R.; Muscat, A. J. Kinetics and Mechanism for the Reaction of Hexaflfluoroacetylacetone with CuO in Supercritical Carbon Dioxide. *J. Am. Chem. Soc.* **2008**, *130*, 16659−16668.
(63) Sun, S.; Zhang, X.; Sun, Y.; Yang, S.; Song, X.; Yang, Z. Hierarchical CuO nanoflowers: water-required synthesis and their application in a nonenzymatic glucose biosensor. *Phys. Chem. Chem. Phys.* **2013**, *15*, 10904−10913.
(64) Frindy, S.; Kadib, A. E.; Lahcini, M.; Primo, A.; Garcia, H. Isotropic and oriented copper nanoparticles supported on graphene as aniline guanylation catalysts. *ACS Catal.* **2016**, *6*, 3863−3869.
(65) Hou, Z.; Chai, R.; Zhang, M.; Zhang, C.; Chong, P.; Xu, Z.; Li, G.; Lin, J. Fabrication and Luminescence Properties of One-Dimensional $CaMoO_4$: Ln^{3+} (Ln = Eu, Tb, Dy) Nanofibers via Electrospinning Process. *Langmuir* **2009**, *25*, 12340−12348.
(66) Ghobashy, M. M.; Alshangiti, D. M.; Alkhursani, S. A.; Al-Gahtany, S. A.; Shokr, F. S.; Madani, M. Improvement of In Vitro Dissolution of the Poor Water-Soluble Amlodipine Drug by Solid Dispersion with Irradiated Polyvinylpyrrolidone. *ACS Omega* **2020**, *5*, 21476−21487.
(67) Huang, T.; Shao, Y.-W.; Zhang, Q.; Deng, Y.-F.; Liang, Z.-X.; Guo, F.-Z.; Li, P.-C.; Wang, Y. Chitosan-cross-linked graphene oxide/carboxymethyl cellulose aerogel globules with high structure stability in liquid and extremely high adsorption ability. *ACS Sustainable Chem. Eng.* **2019**, *7*, 8775−8788.
(68) Song, S. J.; Wang, Y. L.; Xie, J.; Sun, B. H.; Zhou, N. L.; Shen, H.; Shen, J. Carboxymethyl Chitosan Modified Carbon Nanoparticle for Controlled Emamectin Benzoate Delivery: Improved Solubility, pH-Responsive Release, and Sustainable Pest Control. *ACS Appl. Mater. Interfaces* **2019**, *11*, 34258−34267.
(69) Sahne, F.; Mohammadi, M.; Najafpour, G. D. Single-Layer Assembly of Multifunctional Carboxymethylcellulose on Graphene

Oxide Nanoparticles for Improving in Vivo Curcumin Delivery into Tumor Cells. *ACS Biomater. Sci. Eng.* **2019**, *5*, 2595−2609.
(70) Tanguy, N. R.; Wu, H.; Nair, S. S.; Lian, K.; Yan, N. Lignin cellulose nanofibrils as an electrochemically functional component for high-performance and flexible supercapacitor electrodes. *ChemSusChem* **2021**, *14*, 1057−1067.

https://doi.org/10.1021/acsomega.1c02031
ACS Omega 2021, 6, 18157−18168